First-principles study of ionic oxygen mobility of Sr-containing LaAlO$_3$ perovskite

First-principles study of ionic oxygen mobility of Sr-containing LaAlO₃ perovskite

Norge Cruz Hernández[1]**, Javier Fernández Sanz**[2] **and**
Luis Javier Alvarez[3,4]

[1] Departamento de Física Aplicada I, Escuela Universitaria Politécnica,
Universidad de Sevilla, E-41011 Sevilla, Spain
[2] Departamento de Química Física, Facultad de Química, Universidad de Sevilla,
E-41012 Sevilla, Spain
[3] Laboratorio de Simulación, Instituto de Matemáticas, Unidad Cuernavaca, Universidad
Nacional Autónoma de México, AP 273-3 Admon. 3, Cuernavaca, Morelos 62251, Mexico

E-mail: lja@matcuer.unam.mx

Abstract
The fundamental phenomena underlying the electrical conduction properties of Sr-containing
LaAlO₃ perovskites are studied through DFT simulations. The most energetically favourable
substitution sites for Sr in the LaAlO₃ lattice and the energetic barriers for oxygen diffusion
were calculated. *Ab initio* molecular dynamics was used to investigate the onset of oxygen
transport. Experimental characterization of this material has suggested the existence of
undercoordinated Al atoms upon substitution of La with Sr. Our results confirm the existence of
four- (Al^{IV}) and fivefold (Al^{V})-coordinated Al at the expense of the amount of
sixfold-coordinated ones (Al^{VI}), and explain the appearance of a small peak at 66 ppm in the
^{27}Al NMR spectrum.

(Some figures in this article are in colour only in the electronic version)

1. Introduction

Materials with high ion diffusivity are attracting the attention of many researchers because of their potential technological applications. Probably the most important application for which these materials are prepared is as solid oxide fuel cells (SOFC). In addition, mixed conducting oxides stable at high temperature in low Po₂ can be used in a number of applications such as oxygen separation membranes in molten metals and H₂ or CO generation by direct thermal splitting. One of the most important properties of perovskites is the electrical conductivity. Perovskites are among the best oxygen conductors and their conductivity can be enhanced with a number of procedures. These procedures include the addition of dopants [1], substitution of both La and Al by Sr and Mn, respectively, in the case of LaAlO₃, formation

of multilayers [2], nonstoichiometry, etc. Doped perovskites, which possess a high electronic conductivity in addition to the ionic one, are considered for use as electrodes in SOFC and as oxygen-selective membranes; for example, strontium-doped lanthanum manganese oxide, $La_{1-y}Sr_yMnO_{3-y/2}$ is a standard cathode material for SOFC applications operating at temperatures around 1000 °C. Because of the wide spectrum of applications it is necessary to study the factors determining the basic phenomena that give rise to oxygen mobility and the detailed mechanisms of the onset of diffusion in a systematic way. Theoretical work in this direction has seldom been done after the pioneering work of Kilner and Brook [3]. Recently classical molecular dynamics simulations have been performed in similar systems [4]. In this work we present a density functional theory analysis of a previously studied material [5], $La_{0.8}Sr_{0.2}AlO_{2.9}$, which was originally chosen because of its high ionic conductivity.

[4] Author to whom any correspondence should be addressed.

2. Method

In order to simulate the perovskite structure we have used VASP code [6–9]. This code employs a basis set of plane waves to solve the Kohn–Sham equations of the density functional theory (DFT) in a periodic system, where a repeated cubic cell is used to represent the bulk. We have used the generalized gradient approximation (GGA) functional built from the Perdew and Zunger [10] local functional, the interpolation formula of Vosko *et al* [11] and the gradient corrections by Perdew *et al* [12]. The interaction between the valence electrons and the core was described by the projected augmented wave (PAW) method [13] in the implementation of Kresse and Joubert [14]. Scalar relativistic effects are included in these potentials, which are necessary for the correct description of the electronic structure when heavy atomic species (like Sr and La) are involved. We considered the Al (3s, 3p), Sr (4s, 4p, 5s), O (2s, 2p) and La (4p, 5s, 6d) electrons as valence states, while the remaining electrons were kept frozen as core states. The number of plane waves in VASP is controlled by a cutoff energy, which in our calculations was set to $E_{\text{cut}} = 500$ eV.

Cell parameters were optimized for $LaAlO_3$ on a system consisting of eight unit cells arranged within a cube ($2 \times 2 \times 2$). In this way, optimizations were performed using a conjugated gradient technique in which the iterative relaxation of atomic positions was stopped when the forces on the atoms were less than 0.01 eV Å^{-1}. For all geometry optimization calculations a $2 \times 2 \times 2$ mesh of k-points was used to sample the reciprocal space. The optimized cell parameter for the parent perovskite was 7.636 Å, in agreement with the reported experimental value of 7.580 Å [15]. In a second set of calculations, substitutions of La by Sr were performed in such a way that two lanthanum cations were substituted by two strontium cations and one O anion was removed to preserve the electroneutrality of the system. In each La–Sr substitution and O removal, cell parameters were optimized, obtaining values around 7.66 Å, which increased around 0.3% with respect to the calculated value of the parent $LaAlO_3$ perovskite. All possible substitutions were explored through the determination of the cohesion energy. The substitution of two La cations by two Sr cations yields $La_{0.75}Sr_{0.25}AlO_{3-0.125}$, which is the closest possible configuration to the experimental one reported in [5].

There are three possible configurations upon substitution of two La by two Sr taking into account the symmetry of the system, labelled S_1, S_2 and S_3. For each of these substitutions there should be an oxygen vacancy due to the removal needed to have a stoichiometric system. Therefore, once a substitution is made there are a number of possibilities for the removal of oxygen. Figure 1 shows the nine possible configurations for a system of this size. The labels in the figure correspond to the number of possible substitutions, S_i, and the possible vacancy locations, V_j, for the corresponding S_i.

3. Results and discussion

The first result we have obtained is that all substitution sites differ in stabilization energy by less than 0.39 eV, as can be

seen from figure 1 where the relative energies have been shown for each representation of the substitutional configurations. The most stable case is the S_1–V_3, while the less stable is the S_2–V_1. As it should be expected, from an electrostatic viewpoint this is the most stable configuration upon changing two +3 charges for two +2 charges.

As has been mentioned earlier, one of the most important properties of this kind of perovskite is their electrical ionic conductivity, which is intimately related to oxygen mobility. This is a motivation to study the energetic barriers that prevent oxygen atoms starting a possible diffusion process. In our model oxygen motion takes place when one oxygen anion tends to go to the vacancy created when substitutions of La by Sr were carried out. The system is transforming continuously, as was observed from the molecular dynamics simulations described below. Transformations occur among the configurations illustrated in figure 1. Because of symmetry reasons the transformation may also be from one configuration to the same one. Two types of moves are possible for the system to go from any configuration to any other possible configuration. The first one is on a straight line joining the occupied site and the vacancy. The other possibility is on a curve around an aluminium cation.

Transformations of substituted structures among themselves were analysed, i.e. $(S_n–V_m) \leftrightarrow (S'_n–V'_m)$. Starting from one of the structures $S_n–V_m$ (figure 1) we performed a transition state search using the climbing image nudged elastic-band approach, as implemented in the VASP program [16, 17] and estimated the activation energies to move one of the oxygen atoms to the neighbouring vacancy. For the case of a straight path only one starting point was used whereas for the curved path three starting points were used. All feasible pathways for all structures were analysed through the calculation of the energy barrier. This analysis yielded a generalized behaviour, which is illustrated only for the most stable case. Figure 2 shows an illustration of the reaction coordinates obtained for the two types of motion. In the case in which hopping takes place on a straight pathway the moving oxygen is in the middle of the upper left of the starting model, whereas the moving oxygen for the curved pathway is in the front of the system. Small light gray spheres (green in the colour version) in the figure show the two oxygen atoms that could move to the vacancy through different pathways to generate an S_1–V_3 self-transformation. Note in the figure that when one oxygen cation moves the other one is kept in its place. The two final stages obtained are equivalent and correspond to the S_1–V_3 configuration. Vacancy positions are indicated in the starting and final configurations with blue labels 'V'.

Thus, the estimated barriers were ∼3 eV and ∼0.5 eV for linear and curved pathways, respectively. We have also found that the energy barriers could change if the sense of the path was reversed for some of the linear cases depending on whether or not there are Sr atoms in the path. For the linear paths oxygen can go through three different environments La–La, La–Sr and Sr–Sr which are essentially equivalent from the energetic point of view and given by the steric hindrance. Regarding the curved paths, the difference in energy for an O atom to move to the neighbouring vacancy also depends on the
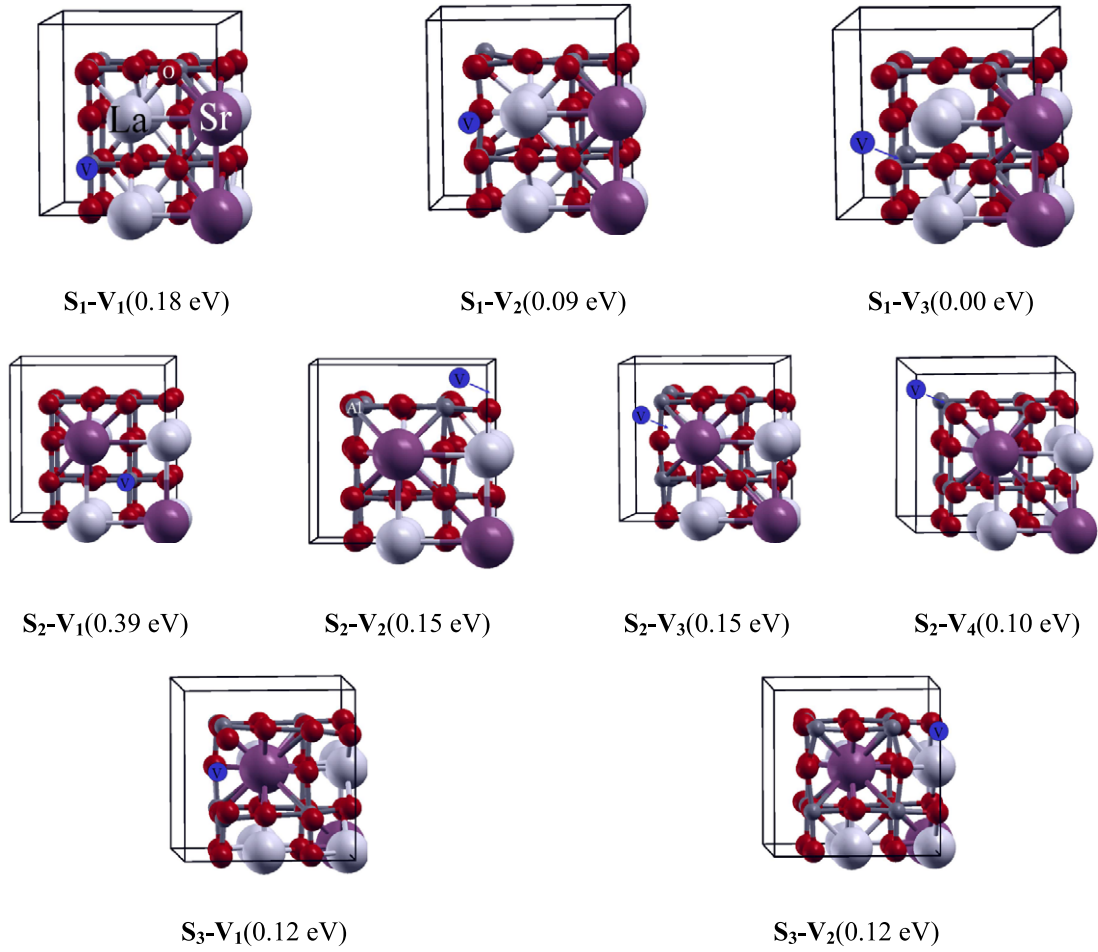
Figure 1. Possible structures obtained after substitution of La by Sr and removal of excess oxygen atoms. S_1, S_2 and S_3 correspond to the three different substituted structures, V_j corresponds to the different locations of vacancies and the small blue circle with a 'V' indicates the position of the vacancy.
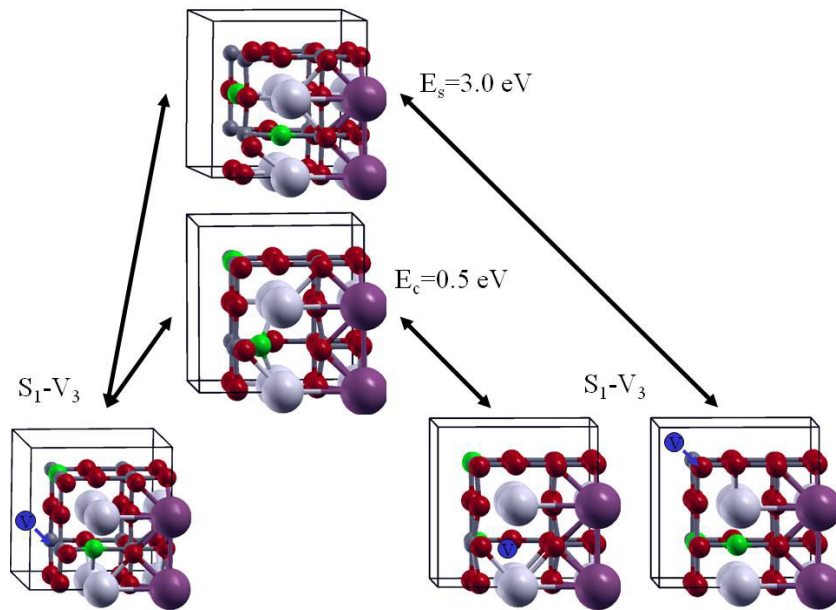

Figure 2. Reaction coordinates for the motion of one oxygen atom to the neighbouring vacancy for both the straight line and curved pathways. Small light gray spheres (green in the colour version) indicate oxygen atoms that move.
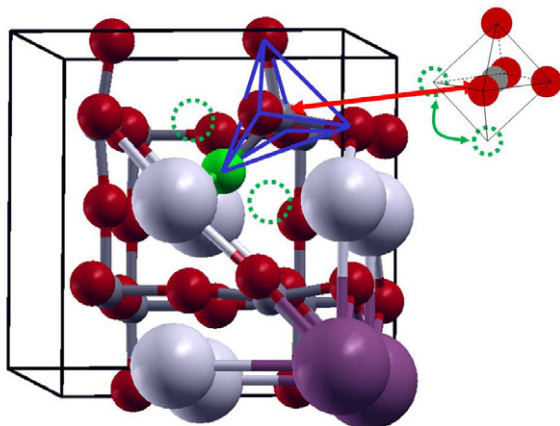
Figure 3. Detailed view of the bi-pyramid structure of the transition state for the curved path.

Figure 4. Time dependence of Al coordination number at 2000 K.

presence of either La or Sr in the path but they are always less than 0.5 eV, which makes them more probable. The transition state for the curved paths looks like a bi-pyramid illustrated in figure 3 which is a snapshot of the configuration given by MD simulations at 300 K described below.

DFT molecular dynamics simulations were performed in the microcanonical ensemble using the periodic model and density functional, as well as reducing the reciprocal space to the Γ point in order to identify the transition state, to demonstrate that undercoordinated Al cations are being created and to calculate the total radial distribution function to be compared to the experimental one. The simulated system was a $4 \times 4 \times 4$ supercell of S_1–V_3 configuration with 48 La, 16 Sr, 64 Al and 184 O atoms. Previous to production runs, rescaling velocities of all particles for thermalization were carried out. These runs were performed for a long enough time in such a way as to achieve thermal equilibrium when temperature control was removed to change to the NVE ensemble. In this way energy fluctuations were less than 10^{-4} of the mean value in the production stage.

As has been mentioned before, the transition energy barrier is less than 0.5 eV, which implies that the local configuration is changing from one state to another. It is worth noting that since our simulations are limited by system size and the short simulated time that can be achieved because of the computational burden, transitions with higher transition energies or low probability, are not observed. This does not mean that they may not occur in the real system. The observed transition must be a short residence time in the transition state. Therefore, aluminium coordination analysis was performed for every configuration given by MD simulations in order to illustrate the fact that oxygen atoms are continuously going back and forth from one vacancy to another through the transition state. Because of the size of the simulated system and the low probability of oxygen migration to be observed at 300 K analyses were performed at 2000 K to improve the mobility of all species. Figure 4 shows the time dependence of the number of Al atoms for the three different coordination numbers that appear along the simulated time of 1 ps. The continuous transition from Al^V to Al^{VI} has a concomitant effect of producing a small number of instantaneous Al^{IV} which are
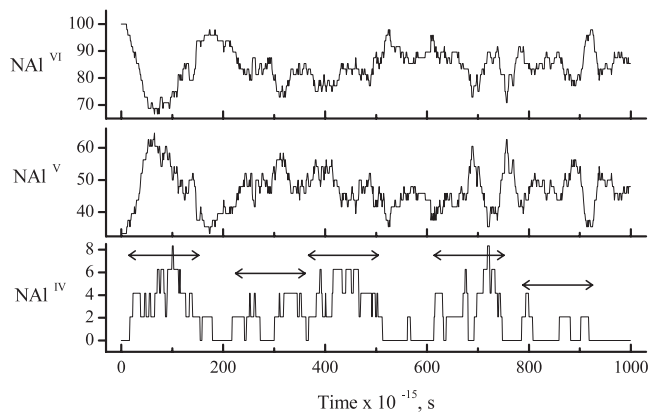
responsible for the appearance of the 66 ppm peak in the ^{27}Al NMR spectrum of [5]. The residence time at the transition state was estimated to be 1.33×10^{-13} s from this graph. In figure 4 there are five arrows indicating the periods of time the transition state was achieved by the simulated system.

The total radial distribution function $G(r)$, obtained from MD simulations, is given by

$$G(r) = 4\pi r \sum_{i=1}^{N_p} c_i g_i(r),$$

where $g_i(r)$ is the pair radial distribution function of the ith pair, c_i are coefficients that depend on the dispersion factors and the partial concentration of each pair of interacting species and N_p is the total number of interacting species. This function is obtained experimentally from the Fourier transform of the structure factor which in turn comes from the x-ray diffractogram. Figure 5 shows the calculated and experimental $G(r)$. The experimental function was obtained for a system very similar to the simulated one. As can be seen there is an excellent agreement that has allowed us to assign the particular pairs that produce the peaks of the total radial distribution function. In the inset of this figure we have included the distribution of distances Al^V–O and Al^{VI}–O to show that they are indistinguishable in the experimental $G(r)$. A Gaussian distribution was fitted to each of the calculated distributions. The number of tetrahedral aluminium atoms is so small that its signal in the x-ray diffraction experiment cannot be distinguished from noise. The MD simulations clearly solve this point.

4. Conclusions

Density functional theory calculations were performed to study the mobility of oxygen in the $La_{0.75}Sr_{0.25}AlO_{3-0.125}$ perovskite, first exploring all the possible substitution sites and associated oxygen vacancies and then calculating the energy barriers that oxygen atoms have to overcome to start moving in the lattice. Molecular dynamics simulations, also within the DFT formalism, were performed to corroborate that mobility of oxygen is as predicted by the static calculations. Three main conclusions can be drawn from our calculations. First, the preferential path of oxygen to jump from one
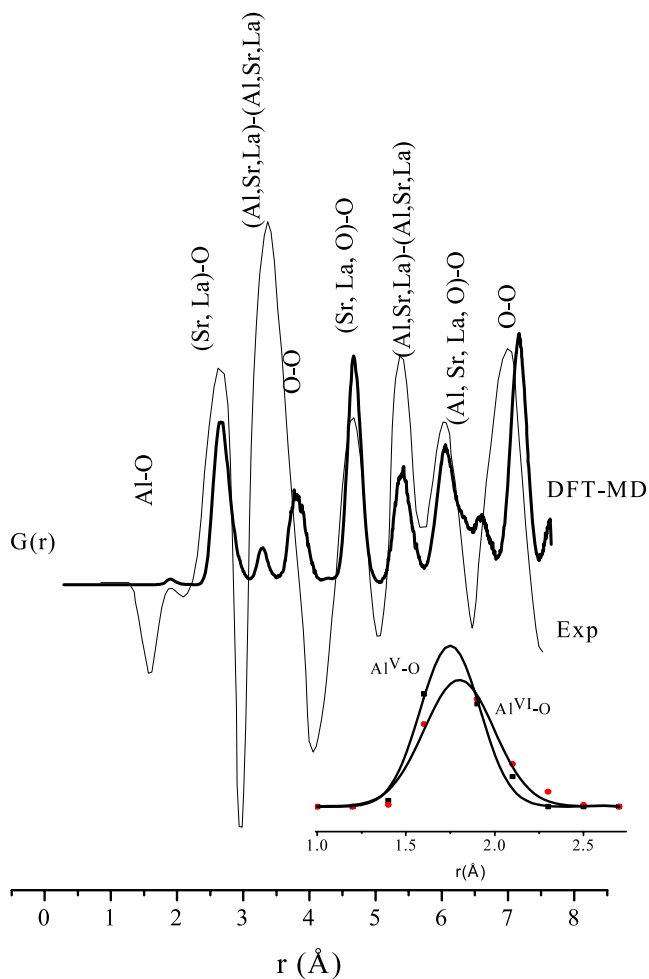
Figure 5. Experimental and calculated total radial distribution functions $G(r)$ of La$_{0.75}$Sr$_{0.25}$AlO$_{3-0.125}$ perovskite.

site to the neighbouring vacancy is a curved one. The straight line joining one site and the vacancy is strongly unfavourable. The experimental peak of the NMR of ^{27}Al at 66 ppm is interpreted as produced by the transition state from one configuration to another since the energy barrier is too low. There is a residence time in the transition state that produces the weak 66 ppm signal of the NMR spectrum. The peaks of the experimental radial distribution

function are assigned based on the total radial distribution function calculated from molecular dynamics simulations and corroborate the previously calculated ones based on classical molecular dynamics simulations [5].

References

[1] Young Park J and Man Choi G 2005 *Solid State Ion.* **176** 2807
[2] Gemming S and Seifert G 2006 *Acta Mater.* **54** 4299
[3] Kilner J A and Brook R J 1982 *Solid State Ion.* **6** 237
[4] Fisher C A J, Yoshiya M, Iwamoto Y, Ishii J, Asanuma M and Yabuta K 2007 *Solid State Ion.* **177** 3425
[5] Lima E, Ibarra-Palos A, Villafuerte-Castrejón M E, Saniger J M, Sánchez-Sánchez J E and Álvarez L J 2008 *Solid State Ion.* **178** 1944
[6] Kresse G and Fruthmuller J 1996 *Comput. Mater. Sci.* **6** 15
[7] Kresse G and Fruthmuller J 1996 *Phys. Rev.* B **54** 11169
[8] Kresse G and Hafner J 1993 *Phys. Rev.* B **48** 13115
[9] Kresse G and Hafner J 1994 *J. Phys.: Condens. Matter* **6** 8245
[10] Perdew J P and Zunger A 1981 *Phys. Rev.* B **23** 5048
[11] Vosko S H, Wilk L and Nusair M 1980 *Can. J. Phys.* **58** 1200
[12] Perdew J P, Chevary J A, Vosko S H, Jackson K A, Pederson M R, Singh D J and Fiolhais C 1992 *Phys. Rev.* B **46** 6671
[13] Blochl P E 1994 *Phys. Rev.* B **50** 17953
[14] Kresse G and Joubert D 1999 *Phys. Rev.* B **59** 1758
[15] Jacobs J P, San Miguel M A and Álvarez L J 1997 *J. Mol. Struct. (Theochem)* **390** 193
[16] Henkelman G and Jónsson H 1999 *J. Chem. Phys.* **111** 7010
[17] http://theory.cm.utexas.edu/vsttools/neb/